

Smooth Feedback Construction Over Spherical Polytopes*

Xiao Tan¹, Soulaïmane Berkane² and Dimos V. Dimarogonas¹

Abstract—In this work, we investigate the partitioning and control problems on the 2–sphere, the set of all unit vectors in \mathbb{R}^3 . Specifically, we present a spherical-polytope-based partitioning for the 2–sphere and then propose a novel approach to construct a feedback control law over a given set of spherical polytopes. Instead of designing the control law directly on the sphere, we propose a smooth atlas on it based on the gnomonic projection. We further show that the gnomonic map projects the spherical polytopes to Euclidean polytopes. Moreover, the kinematics evolving on a spherical polytope can be transformed via feedback into a single integrator in the Euclidean space. Thanks to these properties, control algorithms that were originally developed for polytopes in Euclidean spaces can now be applied to spherical polytopes on the 2–sphere. We conclude this paper by showing a control construction on the sphere with cluttered obstacles.

I. INTRODUCTION

The motivation for studying the dynamical systems evolving on a 2–sphere, the set of all unit vectors in \mathbb{R}^3 , comes from two aspects: on the one hand, many practical systems contain state components that are constrained to evolve on the sphere. The rigid-body reduced attitude model is an important example, where only two (instead of three axis) rotational movements are of interest [1]. This model has broad applications in aerospace and robotics, for example, a spacecraft with one axis actuation failure [2]. In these cases, the controlled two degrees of freedom are naturally identified as the 2–sphere. Other applications include the spherical pendulum [3] and the visual tracking task [4].

On the other hand, the underlying configuration space is not diffeomorphic to any Euclidean space, and this nontrivial topology results in interesting and complicated nonlinear dynamics. One well-known theoretical result in this field is that there exists no time-invariant continuous control law that can globally stabilize a state on the sphere [5]. Many control strategies [1], [4], [6] are proposed in the literature by inherently considering the nonlinear manifold characteristics to avoid singularities and ambiguities of other representations, and almost globally asymptotic stability is generally achieved.

One more challenging problem is to control dynamical systems that the states are constrained to ‘local’ regions of

the 2–sphere. This is motivated by applications where the state can only evolve on a subset of the sphere due to safety reasons. For example, the attitude maneuvering of a space telescope observing galaxies requires to actively avoid the direct exposure to sun [7]. The constrained attitude problem is generally solved by considering the full attitude model (i.e., rotational space $SO(3)$, quaternion representation, etc) [8]–[10]. However, in an under-actuated scenario, solutions for a full attitude is not applicable to a reduced attitude model. There exist very few results that deal with the constrained control problem on the 2–sphere. [11] solves the problem by extending a barrier-function based method on manifolds where an online state-dependent quadratic programming is incorporated. [12] uses a stereographic projection strategy that transforms conic constraints on the n –spheres to spherical polytope shapes of constraints on the sphere here.

In this work, we consider the constrained control problem on the 2–sphere within the framework of partitioning, planning and control modules [10]. More specifically, we propose a spherical polytope decomposition of the feasible region and develop control laws over these spherical polytopes. The spherical-polytope based partitioning is directly performed on the 2–sphere without resorting to any local parameterizations. Compared to [11], [12], our method can be applied to general shapes of feasible regions. We further present a novel approach to construct a feedback control law that enables two state behaviors over a set of spherical polytopes: the transition between two adjacent spherical polytopes and the convergence to a goal state. The control construction relies on the gnomonic projection that maps spherical polytopes into polytopes in \mathbb{R}^2 and, more importantly, the transformed dynamics can be linearized to a single integrator via feedback. Thanks to these nice properties, control algorithms [13], [14] that were originally designed for Euclidean polytope navigation can now be utilized for spherical polytopes. We conclude this paper with two numerical examples.

II. NOTATIONS AND SPHERICAL POLYTOPE PARTITIONING

The set of real, non-negative real, and positive integer numbers are denoted as $\mathbb{R}, \mathbb{R}_{\geq}, \mathbb{N}$, respectively. \mathbb{R}^n denotes the n -dimensional Euclidean space. For any vectors $\mathbf{x}, \mathbf{y} \in \mathbb{R}^n$, their inner product is defined as $\mathbf{x} \cdot \mathbf{y} := \sqrt{\mathbf{x}^\top \mathbf{y}}$. The 2-norm of a vector \mathbf{x} is $\|\mathbf{x}\|_2 := \sqrt{\mathbf{x}^\top \mathbf{x}}$. $I_n, n \in \mathbb{N}$ is the n -dimensional identity matrix; $\mathbf{0}_{n \times 1}$ is a n -dimensional vector with all entries zero, and $\mathbf{e}_3 = (0, 0, 1)$ is a vector in \mathbb{R}^3 . The map $[(\cdot)]_{\times} : \mathbb{R}^3 \rightarrow \mathbb{R}^{3 \times 3}$ for any $\mathbf{x} = (x_1, x_2, x_3)$ is

*This work was supported by the H2020 ERC Starting Grant BUCOPH-SYS, the EU H2020 Research and Innovation Programme under GA No. 731869 (Co4Robots), the SSF COIN project, the Swedish Research Council (VR) and the Knut och Alice Wallenberg Foundation.

¹Xiao Tan and Dimos V. Dimarogonas are with the Division of Decision and Control Systems, KTH Royal Institute of Technology, Stockholm, Sweden. xiaotan@kth.se, dimos@kth.se

²Soulaïmane Berkane is with Département d’informatique et d’ingénierie, Université du Québec en Outaouais, Québec, Canada. soulaïmane.berkane@uqo.ca

explicitly defined as $[\mathbf{x}]_{\times} = \begin{pmatrix} 0 & -x_3 & x_2 \\ x_3 & 0 & -x_1 \\ -x_2 & x_1 & 0 \end{pmatrix}$.

Let \mathbb{S}^2 denote the unit sphere $\mathbb{S}^2 := \{\mathbf{x} \in \mathbb{R}^3 : \|\mathbf{x}\|_2 = 1\}$. The tangent space to \mathbb{S}^2 at a given point \mathbf{x} is given by $\mathcal{T}_{\mathbf{x}}\mathbb{S}^2 = \{\mathbf{y} \in \mathbb{R}^3 : \mathbf{y}^{\top}\mathbf{x} = 0\}$. Let $\mathbf{x}, \mathbf{y} \in \mathbb{S}^2$. The *spherical distance* is defined as $d_S(\mathbf{x}, \mathbf{y}) := \arccos(\mathbf{x}^{\top}\mathbf{y})$, denoting the length of the shortest curve, i.e., geodesics, on \mathbb{S}^2 between \mathbf{x} and \mathbf{y} . A pair of points \mathbf{x}, \mathbf{y} of \mathbb{S}^2 is said to be *proper* if and only if $\mathbf{x} \neq \mathbf{y}, \mathbf{x} \neq -\mathbf{y}$. If the pair \mathbf{x}, \mathbf{y} is proper, then there exists a unique shortest curve, i.e., geodesic segment, in \mathbb{S}^2 joining \mathbf{x} to \mathbf{y} , denoted by $\text{seg}(\mathbf{x}, \mathbf{y})$. An interesting property is that a geodesic segment of \mathbb{S}^2 is an arc of a great circle [15]. Here a *great circle* of \mathbb{S}^2 is the intersection of \mathbb{S}^2 with a plane passing through the center of the sphere. A subset C of \mathbb{S}^2 is *convex* if and only if for each pair of proper points \mathbf{x}, \mathbf{y} in C , the geodesic segment $\text{seg}(\mathbf{x}, \mathbf{y})$ is contained in C . The *convex hull* of a subset S of X , where X is a metric space, is the intersection of all the convex subsets of X containing S . A set S is called *connected* if for every pair of points $p, q \in S$, there exists a continuous map $f : [0, 1] \rightarrow S$ such that $f(0) = p, f(1) = q$.

A *spherical polytope* P in \mathbb{S}^2 is a convex subset of \mathbb{S}^2 such that P has only finitely many vertices; P is the convex hull of its vertices; and any pair of distinct points in P is proper [15]. Given a finite set of points $\{\mathbf{x}_i\}$ that lie in a hemisphere $U_{\mathbf{a}} := \{\mathbf{x} \in \mathbb{S}^2 : \mathbf{a}^{\top}\mathbf{x} > 0\}$ for some vector $\mathbf{a} \in \mathbb{S}^2$, the spherical polytope is then $\text{Conv}(\{\mathbf{x}_i\})$, where $\text{Conv}(\cdot)$ is a function that gives the convex hull of all its elements. Every spherical polytope P can be written as $P = \{\mathbf{x} \in \mathbb{S}^2 : \mathbf{k}_i^{\top}\mathbf{x} \geq 0\}$, where $\mathbf{k}_i \in \mathbb{S}^2, i = 1, 2, \dots, n$.

A finite collection of spherical polytopes $\mathcal{P} = \{P_i\}$ is called a *spherical polytope partitioning* on \mathbb{S}^2 if 1) the interiors of any spherical polytopes $P_i, P_j \in \mathcal{P}$ are mutually disjoint; 2) the union of the spherical polytopes in \mathcal{P} is \mathbb{S}^2 . One common example of a spherical polytope partitioning is the soccer ball, where each spherical polytope is bounded by 5 or 6 geodesic segments.

III. CONTROL PROBLEM FORMULATION

In this work, we consider a dynamical system whose state evolves on the 2-sphere \mathbb{S}^2

$$\dot{\mathbf{x}} = \Pi(\mathbf{x})\mathbf{u} \quad (1)$$

where $\mathbf{x} \in \mathbb{S}^2$ is the state, $\mathbf{u} \in \mathbb{R}^m$ is the control input, $\Pi : \mathbb{S}^2 \rightarrow \mathbb{R}^{3 \times m}$ is a smooth matrix-valued function that projects \mathbf{u} onto the tangent space $\mathcal{T}_{\mathbf{x}}\mathbb{S}^2$. We assume that the system (1) is fully-actuated. That is,

Assumption 1. For all $\mathbf{x} \in \mathbb{S}^2$, $\text{Im}(\Pi(\mathbf{x})) = \mathcal{T}_{\mathbf{x}}\mathbb{S}^2$.

Since $\dim(\mathcal{T}_{\mathbf{x}}\mathbb{S}^2) = 2$, Assumption 1 implies $m \geq 2$.

One well-known example of (1) is the reduced attitude kinematic model $\dot{\mathbf{x}} = [\mathbf{x}]_{\times}\mathbf{u}$ [1], where \mathbf{x} denotes a fixed unit vector in the inertia frame resolved in the body frame, and $\mathbf{u} \in \mathbb{R}^3$ is the angular velocity expressed in the body frame.

Many applications need the states to evolve only in a subset of the 2-sphere due to safety reasons. For example, the attitude maneuvering for a space telescope may be

required to perform in a small feasible region. In general, with a spherical polytope partitioning \mathcal{P} , the feasible region can be approximated by a subset of \mathcal{P} . In this case, we need to constrain the state behavior on a given set of spherical polytopes. This constrained control problem on the 2-sphere is described in Problem 1.

Problem 1. (Control over spherical polytopes) Given a spherical polytope partitioning \mathcal{P} . Let \mathcal{P}' be a subset of \mathcal{P} , $M := \cup_i P_i, \forall P_i \in \mathcal{P}'$, and $\mathbf{x}_g \in M$. Assume that M is connected. Construct a feedback control input \mathbf{u} such that

- 1) all integral curves starting in M and under the control input \mathbf{u} are smooth.
- 2) for all initial states $\mathbf{x}(0) \in M$, $\mathbf{x}(t) \in M$ for all $t \geq 0$ and $\mathbf{x}(t)$ reaches \mathbf{x}_g asymptotically.

In what follows, we call P_i an *intermediate spherical polytope* if $P_i \in \mathcal{P}', \mathbf{x}_g \notin P_i$; and P_i is the *goal spherical polytope* when $\mathbf{x}_g \in P_i$.

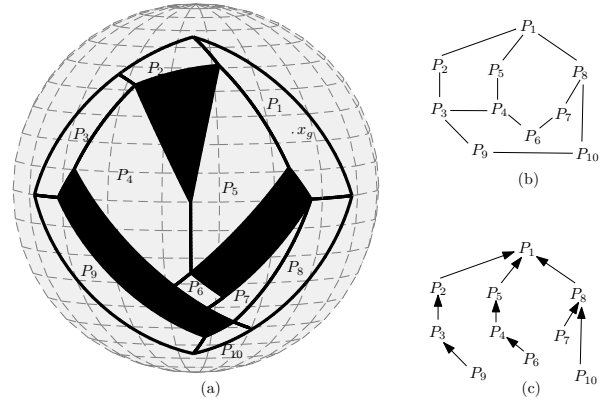


Fig. 1. (a) A subset of \mathbb{S}^2 decomposed into spherical polytopes. The black regions are the obstacles in the environment. (b) The corresponding connectivity graph, which is constructed with spherical polytopes to be the nodes and the adjacency relations to be the edges. (c) A path over all the spherical polytopes that ultimately leads to the goal one.

We solve Problem 1 in two steps: 1) find a path over spherical polytopes that leads to the goal spherical polytope, 2) construct a feedback control law that enables every transition in the path. In the first step, given spherical polytopes $\{P_i\}$ and the goal state \mathbf{x}_g as shown in Fig. 1(a), a search algorithm could be utilized to find a sequence of adjacent spherical polytopes that leads to the spherical polytope containing \mathbf{x}_g , see Fig. 1(b)(c). Note that a path with minimal hops to the goal polytope is chosen here. Further modifications could be done in this step by taking the size or the traveling time into account. The second step is to construct a feedback control law for each spherical polytope (Problem 2) with a smooth blending between successive spherical polytopes (Problem 3).

Problem 2. (control over one spherical polytope) Given a spherical polytope P . Construct a feedback control input \mathbf{u} such that

- 1) all integral curves starting in P and under the control input \mathbf{u} are smooth in P .

- 2) if P is an intermediate spherical polytope, then all integral curves starting in P stay in P until they reach the exit face seg_{e_x} in finite time;
- 3) if P is the goal spherical polytope, then all integral curves starting in P stay in P and asymptotically converge to the goal point x_g .

Problem 3. (smooth blending condition) For any two successive spherical polytopes $P, P' \in \mathcal{P}$, the feedback control input $u(x)$ should be smooth for $x \in \text{seg}$, where seg is the shared boundary of P, P' .

In the following sections, we discuss some properties of gnomonic projection that will facilitate the construction of feedback control laws on spherical polytopes and then proceed to solving Problems 2~3.

IV. PROPERTIES OF GNOMONIC PROJECTION

A. Gnomonic projection

For a point $a \in \mathbb{S}^2$, the gnomonic projection projects a point x on the hemisphere $U_a := \{x \in \mathbb{S}^2 : a^\top x > 0\}$ from the center of the sphere o to the unique point x' on the plane $S_a = \{x \in \mathbb{R}^3 : a^\top x = 1\}$ that is tangent to \mathbb{S}^2 at a [16]. An illustration of the gnomonic projection when $a = e_3$ is shown in Fig. 2.

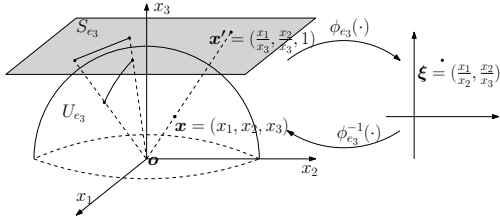


Fig. 2. Gnomonic projection of a point/geodesic segment on a hemisphere onto a plane tangent to \mathbb{S}^2 .

For any point $x \in U_a$, the corresponding point x' under the gnomonic projection lies both on the radial line ox and the plane S_a . Thus, $x' = \frac{x}{a^\top x}$. We define the gnomonic projection mapping for $a \in \mathbb{S}^2$ to be $\phi_a : x \in U_a \mapsto \xi \in \mathbb{R}^2$

$$\phi_a(x) := J_2 R_a \frac{x}{a^\top x}, \quad (2)$$

where $J_2 := [I_2 \quad \mathbf{0}_{2 \times 1}]$, R_a is a matrix that provides a rotation along axis $[a]_\times e_3$ with angle $d_S(a, e_3)$, and is explicitly given by $R_a = I_3 + \sin(d_S(a, e_3))[a]_\times e_3 + (1 - \cos(d_S(a, e_3)))[a]_\times e_3^2$. For any given $a \in \mathbb{S}^2$, R_a is a constant orthogonal matrix. Geometrically speaking, R_a rotates $x' = \frac{x}{a^\top x}$ from the plane S_a to the point $R_a \frac{x}{a^\top x}$ on the plane S_{e_3} . Thus, the third entry of the point $R_a \frac{x}{a^\top x}$ is 1. Note that $\phi_a(\cdot)$ is well-defined on U_a thanks to the fact that for any $x \in U_a$, $a^\top x > 0$.

It can be verified that the inverse map $\phi_a^{-1} : \xi \in \mathbb{R}^2 \mapsto x \in U_a$ is

$$\phi_a^{-1}(\xi) := \frac{R_a^\top (J_2^\top \xi + e_3)}{\sqrt{\xi^\top \xi + 1}} \quad (3)$$

From (2) and (3), ϕ_a and ϕ_a^{-1} are continuous, and then ϕ_a is a homeomorphism. Thus, (U_a, ϕ_a) is a chart for \mathbb{S}^2 .

Proposition 1. A collection of charts $\mathcal{A} = \{(U_a, \phi_a)\}_{a \in \mathbb{S}^2}$ is a smooth atlas for \mathbb{S}^2 .

Proof. See Appendix.

B. The gnomonic projection of spherical polytopes

In addition to providing a smooth atlas for \mathbb{S}^2 , the gnomonic projection projects spherical polytopes from \mathbb{S}^2 to Euclidean polytopes in \mathbb{R}^2 as shown in this subsection.

Since any spherical polytope is contained in a hemisphere [15], without loss of generality, we consider a spherical polytope P that is contained in $U_{e_3} = \{x \in \mathbb{S}^2 : e_3^\top x > 0\}$. Consider also the gnomonic projection mapping $\phi_{e_3}(x) = J_2 \frac{x}{e_3^\top x}$ with the inverse map $\phi_{e_3}^{-1}(\xi) = \frac{J_2^\top \xi + e_3}{\sqrt{1 + \xi^\top \xi}}$. Here $\phi_{e_3}(\cdot)$ is well-defined on U_{e_3} as discussed (as a special case $a = e_3$). This scenario is illustrated in Fig. 2.

Proposition 2. For any proper pair $x_1, x_2 \in U_{e_3}$, the gnomonic projection of $\text{seg}(x_1, x_2)$ forms a line in \mathbb{R}^2 .

Proof. Let x_3 be a unit vector that is orthogonal to x_1, x_2 , and $x' \in \mathbb{R}^3$ be the mapped point of $x \in \text{seg}(x_1, x_2)$. As the geodesics on \mathbb{S}^2 are great circles, for any $x \in \text{seg}(x_1, x_2)$, we have x_1, x_2, o, x are on the same plane $S_{x_1 o x_2} := \{y \in \mathbb{R}^3 : x_3^\top y = 0\}$. In view of $x' = \frac{x}{e_3^\top x}$, we have $x_3^\top x' = 0$, i.e., x' also lies on the plane $S_{x_1 o x_2}$. Recall that x' lies on the plane $S_{e_3} = \{y \in \mathbb{R}^3 : e_3^\top y = 1\}$. Note again that $e_3 \nparallel x_3$ (otherwise, we derive $e_3^\top x_1 = 0$, which violates the fact that $x_1 \in U_{e_3}$), and x' thus lies in the intersection of two nonparallel planes, i.e., a line. \square

Proposition 3. Given a spherical polytope $P \subset U_{e_3}$, the gnomonic projection of the spherical polytope is a Euclidean polytope in \mathbb{R}^2 .

Proof. Let the spherical polytope P bounded by m geodesic segments, denoted as $P = \{x \in \mathbb{S}^2 : k_i^\top x \geq 0 \text{ for } i = 1, 2, \dots, m\}$. Correspondingly, for any point $x \in P \subset U_{e_3}$, we have $e_3^\top x > 0$, which leads to $k_i^\top \frac{x}{e_3^\top x} \geq 0$ for all $i = 1, 2, \dots, m$. By applying the identity $I_3 = J_2^\top J_2 + e_3 e_3^\top$ and the projected point $\xi = J_2 \frac{x}{e_3^\top x}$, we have $k_i^\top \frac{x}{e_3^\top x} \geq 0 \Leftrightarrow k_i^\top (J_2^\top J_2 + e_3 e_3^\top) \frac{x}{e_3^\top x} \geq 0 \Leftrightarrow (J_2 k_i)^\top J_2 \frac{x}{e_3^\top x} + e_3^\top k_i \frac{e_3^\top x}{e_3^\top x} \geq 0 \Leftrightarrow (J_2 k_i)^\top \xi + e_3^\top k_i \geq 0$ for $i = 1, 2, \dots, m$. This forms m linear inequality constraints on $\xi \in \mathbb{R}^2$. Thus, the region subject to these constraints forms a convex polytope in \mathbb{R}^2 . \square

Consider a spherical polytope $P = \text{Conv}(\{x_i\})$ in \mathbb{S}^2 , where the vertices x_i are contained in U_a , $a \in \mathbb{S}^2$. With the projected points $\xi_i = \phi_a(x_i)$, the corresponding projection is $Q = \text{Conv}(\{\xi_i\})$ in \mathbb{R}^2 with vertices $\{\xi_i\}$.

C. Mapping of the dynamics and feedback linearization

In this subsection we investigate the projected dynamics in the Euclidean space. To do so, we consider the change of state variable $\xi = \phi_a(x)$, $x \in U_a$. In view of (1), the derivative of ξ with respect to time is given by

$$\dot{\xi} = \nabla \phi_a(x) \dot{x} = \nabla \phi_a(x) \Pi(x) u := \Theta_a(x) u \quad (4)$$

where $\nabla\phi_{\mathbf{a}}(\mathbf{x})$ denotes the Jacobian matrix of $\phi_{\mathbf{a}}(\cdot)$. From (2), the Jacobian matrix is given by

$$\nabla\phi_{\mathbf{a}}(\mathbf{x}) = \frac{J_2 R_{\mathbf{a}}(\mathbf{a}^\top \mathbf{x} I_3 - \mathbf{x} \mathbf{a}^\top)}{(\mathbf{a}^\top \mathbf{x})^2} \quad (5)$$

Lemma 1. *If Assumption 1 holds, then $\Theta_{\mathbf{a}}(\mathbf{x}) \in \mathbb{R}^{2 \times m}$ has full row rank for all $\mathbf{x} \in U_{\mathbf{a}}$ and all $\mathbf{a} \in \mathbb{S}^2$.*

Proof. Note that since $\phi_{\mathbf{a}}(\cdot)$ is a diffeomorphism, its Jacobian matrix is full rank and therefore $\text{rank}(\nabla\phi_{\mathbf{a}}(\mathbf{x})) = 2$ for all $\mathbf{x} \in U_{\mathbf{a}}$. Specifically, By the rank-nullity theorem, we have $\dim(\ker(\nabla\phi_{\mathbf{a}}(\mathbf{x}))) = 1$. Observe that

$$\begin{aligned} \nabla\phi_{\mathbf{a}}(\mathbf{x})\mathbf{x} &= \frac{J_2 R_{\mathbf{a}}(\mathbf{a}^\top \mathbf{x} I_3 - \mathbf{x} \mathbf{a}^\top)}{(\mathbf{a}^\top \mathbf{x})^2} \mathbf{x} \\ &= \frac{J_2 R_{\mathbf{a}}(\mathbf{a}^\top \mathbf{x} I_3 \mathbf{x} - \mathbf{x} \mathbf{a}^\top \mathbf{x})}{(\mathbf{a}^\top \mathbf{x})^2} \\ &= 0 \end{aligned} \quad (6)$$

Thus $\ker(\nabla\phi_{\mathbf{a}}(\mathbf{x})) = \{\alpha\mathbf{x} : \alpha \in \mathbb{R}\}$.

Moreover, under Assumption 1, we have $\text{rank}(\Pi(\mathbf{x})) = 2$ and therefore by applying Fact 2.10.14 in [17], one obtains $\text{rank}(\Theta_{\mathbf{a}}(\mathbf{x})) = \text{rank}(\nabla\phi_{\mathbf{a}}\Pi(\mathbf{x}))$

$$\begin{aligned} &= \text{rank}(\Pi(\mathbf{x})) - \dim(\ker(\nabla\phi_{\mathbf{a}}) \cap \text{Im}(\Pi(\mathbf{x}))) \\ &= 2 - \dim(\ker(\nabla\phi_{\mathbf{a}}) \cap \mathbb{T}_{\mathbf{x}}\mathbb{S}^2) \end{aligned}$$

With the fact that $\mathbb{T}_{\mathbf{x}}\mathbb{S}^2 = \{\mathbf{y} \in \mathbb{R}^3 : \mathbf{x}^\top \mathbf{y} = 0\}$, we know $\ker(\nabla\phi_{\mathbf{a}}) \perp \mathbb{T}_{\mathbf{x}}\mathbb{S}^2$, thus $\dim(\ker(\nabla\phi_{\mathbf{a}}) \cap \mathbb{T}_{\mathbf{x}}\mathbb{S}^2) = 0$. Therefore, $\text{rank}(\Theta_{\mathbf{a}}(\mathbf{x})) = 2$ for all $\mathbf{x} \in U_{\mathbf{a}}$. \square

Since $\Theta_{\mathbf{a}}(\mathbf{x})$ is full row rank, its Moore-Penrose pseudo-inverse can be explicitly calculated as

$$(\Theta_{\mathbf{a}}(\mathbf{x}))^\dagger = \Theta_{\mathbf{a}}(\mathbf{x})^\top (\Theta_{\mathbf{a}}(\mathbf{x})\Theta_{\mathbf{a}}(\mathbf{x})^\top)^{-1}. \quad (7)$$

Therefore, we can apply a feedback control law to render the dynamics in (4) to a single integrator, summarized below.

Proposition 4. *Consider the kinematic model (1) evolving on the 2-dimensional hemisphere $U_{\mathbf{a}}$ under the following feedback control law*

$$\mathbf{u} = (\Theta_{\mathbf{a}}(\mathbf{x}))^\dagger \mathbf{v} \quad (8)$$

where $\mathbf{v} \in \mathbb{R}^2$ is a virtual control input. Then, the dynamics of the new variable $\boldsymbol{\xi} = \phi_{\mathbf{a}}(\mathbf{x})$, evolving in the Euclidean space \mathbb{R}^2 , is

$$\dot{\boldsymbol{\xi}} = \mathbf{v}. \quad (9)$$

Proof. This is a straightforward conclusion by substituting (8) into (4) and noticing that $\Theta_{\mathbf{a}}(\mathbf{x})(\Theta_{\mathbf{a}}(\mathbf{x}))^\dagger = I_2$. \square

To sum up, we have shown that 1) the gnomonic projection defines a smooth atlas on the 2-sphere; 2) the spherical polytopes are projected to Euclidean polytopes in \mathbb{R}^2 by the gnomonic projection mapping; and 3) the first-order dynamics on the 2-sphere can be locally mapped into a single integrator in \mathbb{R}^2 . Propositions 2~4 provide us an explicit way to change the state coordinates and map the dynamical system constrained in spherical polytopes to a single integrator system constrained in Euclidean polytopes. Proposition 1 further provides a theoretical foundation that the feedback control laws obtained from different charts can be blended together without loss of smoothness.

V. FEEDBACK LAW CONSTRUCTION OVER SPHERICAL POLYTOPES

In this section, we present how the gnomonic projection tool is integrated with the existing reach control algorithms. We use the algorithm in [14] as a guiding example. First recall the following results from [14].

A. Previous results on vector field construction over Euclidean polytopes

Consider a convex polytope decomposition $\{Q_i\}$ of some connected region in \mathbb{R}^2 with goal state $\boldsymbol{\xi}_g \in \cup_i Q_i$. The goal polytope is the polytope that contains $\boldsymbol{\xi}_g$ and the intermediate polytopes are the polytopes equipped with exit face f_{ex} . The generalized Voronoi diagram (GVD) of a convex polytope is explained in Fig. 3(a).

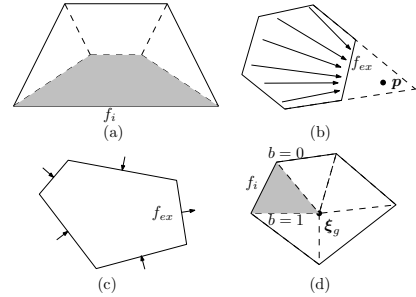


Fig. 3. (a) The generalized Voronoi diagram (GVD) of a convex polytope Q . GVD is formed by partitioning Q into Voronoi regions, which is defined for each face to be the set of points inside the polytope that are closer to that face than to any other face. The GVD surface is the set of points which are equidistant from two or more faces of the polytope. The dash lines are the GVD surfaces, and the shaded region is the (Voronoi) region of the influence of face f_i . (b) An illustration of the cell vector field $V_c(\boldsymbol{\xi}) = \text{unit}(\mathbf{p} - \boldsymbol{\xi})$ by choosing a fixed $\mathbf{p} \in \bar{Q} \setminus Q$, where \bar{Q} is the (possibly unbounded) cell resulting from removal of f_{ex} from Q . (c) An illustration of the face vector field by simply choosing each face vector field perpendicular to its face. (d) The goal polytope. The dash lines are the surfaces of the region partitioning, and the shaded represents the region of influence of face f_i . The interpolating function $b(\boldsymbol{\xi})$ goes from zero on that face to one on the surfaces of the region partitioning. The cell vector field V_c is constructed as $V_c(\boldsymbol{\xi}) = b(\|\boldsymbol{\xi}_g - \boldsymbol{\xi}\|)\text{unit}(\boldsymbol{\xi}_g - \boldsymbol{\xi})$, and V_{f_i} is a smooth unit vector field such that, $V_{f_i}(\boldsymbol{\xi})$ points inwards for every $\boldsymbol{\xi} \in f_i$, and $V_{f_i}(\boldsymbol{\xi}) \cdot (\boldsymbol{\xi}_g - \boldsymbol{\xi}) > 0$ for every $\boldsymbol{\xi}$ in the region of influence of f_i .

For an intermediate polytope Q , a vector field V over Q is constructed by smoothly blending a cell vector field V_c and a face vector field V_{f_i} , i.e.,

$$V(\boldsymbol{\xi}) = \text{unit}(b(\boldsymbol{\xi})V_c(\boldsymbol{\xi}) + (1 - b(\boldsymbol{\xi}))V_{f_i}(\boldsymbol{\xi})) \quad (10)$$

for any point $\boldsymbol{\xi}$ in the region of influence of face f_i , where $\text{unit}(\cdot)$ is a normalization function, ensuring that V is a unit vector field. The interpolating function $b(\boldsymbol{\xi})$ is constructed such that $b(\boldsymbol{\xi}) = 0$ when $\boldsymbol{\xi}$ is on the boundary of Q and $b(\boldsymbol{\xi}) = 1$ when $\boldsymbol{\xi}$ is on the GVD surface. $b(\boldsymbol{\xi})$ has the property that all derivatives equal zero for $\{\boldsymbol{\xi} : b(\boldsymbol{\xi}) = 0\}$ and $\{\boldsymbol{\xi} : b(\boldsymbol{\xi}) = 1\}$. In [14], the authors gave several requirements for constructing the cell vector field V_c and the face vector field V_{f_i} . One simple and efficient way to construct V_c and V_{f_i} is shown in Fig. 3 (b,c).

If Q is the goal polytope, i.e., $\boldsymbol{\xi}_g \in Q$, then the region of influence of a face is shown in Fig. 3 (d). The vector field

on the goal polytope is

$$V(\xi) = b(\xi)V_c(\xi) + (1 - b(\xi))V_{f_i}(\xi) \quad (11)$$

for any point ξ in the region of influence of face f_i . The region of influence of face f_i , the face vector field and cell vector field are explained in Fig.3(d).

Fact 1. Consider the single integrator kinematics $\dot{\xi} = v$ for $\xi \in \mathbb{R}^2$. Given a collection of polytopes $\{Q_i\}$ with $Q_i \subset \mathbb{R}^2$ being connected, and a goal state $\xi_g \in \cup_i Q_i$. With the vector field V in (10)~(11) applied as the control input, the closed-loop system trajectories have the following properties:

- 1) if Q_i is assigned with $f_{ex,i}$, then all integral curves starting in Q_i reach the exit face $f_{ex,i}$ in finite time;
- 2) if Q_i is assigned with the goal point ξ_g , then all integral curves starting in Q_i stay in Q_i and asymptotically converge to ξ_g ;
- 3) all integral curves starting in $\cup_i Q_i$ are smooth, stay inside $\cup_i Q_i$, and asymptotically converge to the goal point ξ_g .

Here we note that the constructed vector field in \mathbb{R}^2 is smooth almost everywhere. More precisely, the constructed vector field is smooth on $\cup_i Q_i$ except for the polytope vertices. Please refer to [14] for more details on the vector field construction in \mathbb{R}^2 .

B. Feedback law construction on spherical polytopes

Consider spherical polytopes $\{P_i\}$ that are connected and jointly lie on one hemisphere U_a (thus all P_i s can be mapped onto \mathbb{R}^2 with one gnomonic projection mapping $\phi_a(\cdot)$ in (2)). Let $P \in \{P_i\}$, seg_{ex} be the exit geodesic segment if P is an intermediate spherical polytope, and x_g be the goal state. A straightforward construction of the feedback control law $u(x)$ for $x \in P$ is stated in Algorithm 1.

Algorithm 1 A feedback law construction over spherical polytopes $\{P_i\}$ given $\cup_i P_i \subset U_a$.

Input: $x, P, \text{seg}_{ex}/x_g, \phi_a(\cdot), \Pi(\cdot)$

- 1: compute $\xi, Q, f_{ex}/\xi_g$ from $x, P, \text{seg}_{ex}/x_g$ by $\phi_a(\cdot)$ in (2)
 - 2: compute v from $\xi, Q, f_{ex}/\xi_g$ by (10)~(11)
 - 3: **return** $u \leftarrow \Theta_a(x)^\dagger v$ where $\Theta_a(x) = \nabla \phi_a \Pi(x)$
-

Let $\{Q_i\}$ be the projected polytopes of $\{P_i\}$ under the mapping ϕ_a . From Fact 1, we know that for single integrator dynamics, with the vector field from [14] applied, any integral curve $s : \mathbb{R}_{\geq} \rightarrow \mathbb{R}^2$ starting from $s(0) \in \cup_i Q_i$ is smooth, contained in $\cup_i Q_i$, and $s(t)$ converges to ξ_g asymptotically. Correspondingly, the integral curve on 2-sphere is $\phi_a^{-1} \circ s : \mathbb{R}_{\geq} \rightarrow \mathbb{S}^2$. As $\phi_a^{-1}(\cdot)$ is a smooth function in the domain of $\cup_i Q_i$ (since $\cup_i Q_i \subset U_a$), any integral curve starting from $\phi_a^{-1}(s(0)) \in \cup_i P_i$ is smooth, contained in $\cup_i P_i$, and $\phi_a^{-1} \circ s(t)$ converges to x_g asymptotically.

However, the constructed control law from Algorithm 1 may lead to a slow motion in the spherical regions that are away from the projection axis a . This is a result of

the length distortion of the gnomonic mapping. One remedy would be to extend the Algorithm 1 with one more step $u \leftarrow u / \|\Pi(x)u\|$. As $\hat{x} = \Pi(x)u$, one obtains $\|\hat{x}\| = 1$ when the extend step is applied, i.e., it generates a unit vector field on $\cup_i P_i$.

Note that the denominator $\|\Pi(x)u\| = \|\Pi(x)(\Theta_a(x))^\dagger v\| > 0$ for any unit norm vector v . This property is due to the fact that $\Pi\Theta_a^\dagger \in \mathbb{R}^{3 \times 2}$ has full column rank (equivalently, $\ker(\Pi\Theta_a^\dagger) = \emptyset$)

$$\begin{aligned} \text{rank}(\Pi\Theta_a^\dagger) &= \text{rank}(\Pi\Theta_a^\top (\Theta_a\Theta_a^\top)^{-1}) = \text{rank}(\Pi\Theta_a^\top) \\ &= \text{rank}(\Pi\Pi^\top \nabla \phi_a^\top) = \text{rank}(\nabla \phi_a \Pi\Pi^\top) \\ &= \text{rank}(\Pi\Pi^\top) - \dim(\ker(\nabla \phi_a) \cap \text{Im}(\Pi\Pi^\top)) \\ &= 2 - \dim(\ker(\nabla \phi_a) \cap T_x \mathbb{S}^n) = 2. \end{aligned}$$

by applying Fact 2.10.14 in [17] again.

One numerical example for the scenario in Fig. 1 is shown in Fig.4. For illustrative purposes, the vector field \hat{x} instead of the feedback law $u(x)$ is shown. This and the following numerical example are performed with a reduced attitude model. Due to space limits, further simulation details are omitted here and can be found online ¹ along with the implementation code.

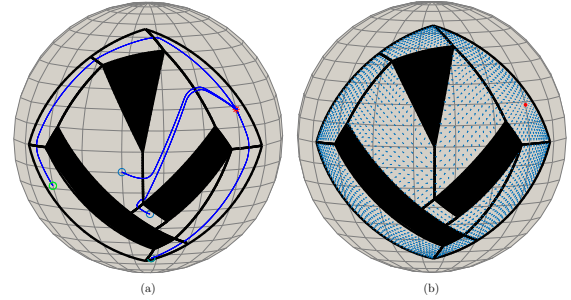


Fig. 4. (a) This plot shows several system trajectories on the 2-sphere under the constructed feedback control laws. The starting states are denoted as circles and the goal state x_g as the star. (b) This plot illustrates the constructed vector field on the given spherical polytopes.

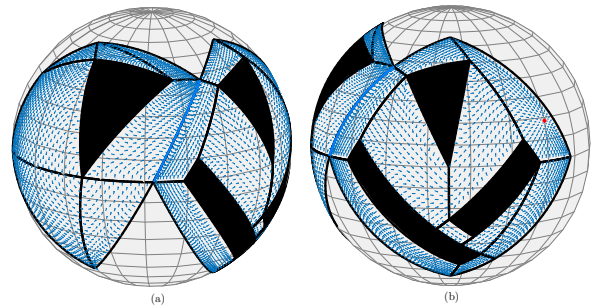


Fig. 5. The two plots illustrate the constructed vector field on an obstacle-cluttered spherical region from two viewpoints. The shared geodesic segment is in blue, and the goal state is in red. The right part of spherical polytopes of seg remains the same as in Fig. 4, while the left half are the extended ones that lie in another chart domain.

A chart transition is needed when constructing a feedback law for spherical polytopes across different charts. As

¹https://github.com/xiaotanKTH/control_2sphere

analyzed in Section IV, for a proper pair $\mathbf{a}, \mathbf{b} \in \mathbb{S}^2$, if the integral curve $s : \mathbb{R}_{\geq} \rightarrow \phi_{\mathbf{a}}(U_{\mathbf{a}} \cap U_{\mathbf{b}})$ is smooth, the corresponding integral curve $\phi_{\mathbf{a}\mathbf{b}} \circ s : \mathbb{R}_{\geq} \rightarrow \phi_{\mathbf{b}}(U_{\mathbf{a}} \cap U_{\mathbf{b}})$ is also smooth. Moreover, for any vector field $V^{\mathbf{a}}$ that is defined to map an element from (a subset of) $\phi_{\mathbf{a}}(U_{\mathbf{a}} \cap U_{\mathbf{b}})$ to \mathbb{R}^2 , the corresponding feedback control law on the 2-sphere is $\Theta_{\mathbf{a}}^{\dagger} V^{\mathbf{a}}$ in view of (8), and the vector field on $\phi_{\mathbf{b}}(U_{\mathbf{a}} \cap U_{\mathbf{b}})$ is $\Theta_{\mathbf{b}} \Theta_{\mathbf{a}}^{\dagger} V^{\mathbf{a}}$ in view of (4). Since $\Theta_{\mathbf{b}}, \Theta_{\mathbf{a}}^{\dagger}$ are smooth matrix-valued functions, if $V^{\mathbf{a}}$ is smooth at $\xi \in \phi_{\mathbf{a}}(U_{\mathbf{a}} \cap U_{\mathbf{b}})$, then $\Theta_{\mathbf{a}}^{\dagger} V^{\mathbf{a}}$ and $\Theta_{\mathbf{b}} \Theta_{\mathbf{a}}^{\dagger} V^{\mathbf{a}}$ are smooth at $\phi_{\mathbf{a}}^{-1}(\xi)$ and $\phi_{\mathbf{a}\mathbf{b}}(\xi)$, respectively.

Here we present one example of constructing smooth feedback laws for spherical polytopes in different chart domains. Without loss of generality, let the spherical polytope $P_1(P_2)$ be in $U_{\mathbf{a}}(U_{\mathbf{b}})$, P_1 successive to P_2 in the sense of the discrete plan (see Fig.1(c)). seg is the shared boundary of P_1 and P_2 . Q_1/Q_2 , $f^{\mathbf{a}}/f^{\mathbf{b}}$ are the projections of P_1/P_2 , seg under the mappings $\phi_{\mathbf{a}}/\phi_{\mathbf{b}}$, respectively. The control law construction over $P_1 \cup P_2$ is stated as follows: 1) for $\mathbf{x} \in P_1 \cup P_2$ and \mathbf{x} is not in the region of influence of $f_{\mathbf{a}}$ in P_1 , the control law is constructed following Algorithm 1; 2) for \mathbf{x} in the region of influence of $f_{\mathbf{a}}$ in P_1 , the control input v at $\xi = \phi_{\mathbf{a}}(\mathbf{x})$ is constructed as $v = b(\xi)V_c(\xi) + (1 - b(\xi))\Theta_{\mathbf{a}}\Theta_{\mathbf{b}}^{\dagger}V_{f_b}^2(\xi)$, where $V_{f_b}^2$ denotes the face vector field of $f^{\mathbf{b}}$ in Q_2 , $b(\xi)$, $V_c(\xi)$, $V_{f_b}^2(\xi)$ are calculated as before. The control input $\mathbf{u} = \Theta_{\mathbf{a}}(\mathbf{x})^{\dagger}v$ where $\Theta_{\mathbf{a}}(\mathbf{x}) = \nabla\phi_{\mathbf{a}}\Pi(\mathbf{x})$. Another numerical example is shown in Fig. 5, where the spherical polytopes are across two chart domains and the vector fields are smoothly blended together.

VI. CONCLUSION

This work presents a spherical-polytope-based partitioning on the 2-sphere and a novel control strategy that regulates the states evolving on a given set of spherical polytopes. The constructed control method relies on the gnomonic projection, for which it is proven that several favorable properties hold: 1) the gnomonic projection defines a smooth atlas on the 2-sphere; 2) the spherical polytopes are projected to Euclidean polytopes in \mathbb{R}^2 ; and 3) the first-order dynamics on 2-sphere can be locally mapped into a single integrator in \mathbb{R}^2 via feedback linearization. Thanks to these properties, algorithms that were originally designed for polytopes in the Euclidean space can be used to construct the feedback laws over the spherical polytopes. Two numerical examples are illustrated utilizing the feedback control algorithm from [14].

The future work involves applying the spherical-polytope partitioning and gnomonic projection tools to under-actuated second-order dynamical systems evolving on higher dimensional spheres. Another direction would be to explore more complex behavior specifications, e.g., attitude maneuvers with temporal logic tasks.

APPENDIX

Proof of Proposition 1. Firstly, $\cup_{\mathbf{a} \in \mathbb{S}^2} U_{\mathbf{a}} = \mathbb{S}^2$ is trivial since for any point $\mathbf{p} \in \mathbb{S}^2$, \mathbf{p} must lie in $U_{\mathbf{p}}$. Consider a proper pair of points $\mathbf{a}, \mathbf{b} \in \mathbb{S}^2$ (thus $U_{\mathbf{a}} \cap U_{\mathbf{b}} \neq \emptyset$ from definition). The overlap map $\phi_{\mathbf{a}\mathbf{b}} := \phi_{\mathbf{b}} \circ \phi_{\mathbf{a}}^{-1}$ from

$\phi_{\mathbf{a}}(U_{\mathbf{a}} \cap U_{\mathbf{b}})$ to $\phi_{\mathbf{b}}(U_{\mathbf{a}} \cap U_{\mathbf{b}})$ can be explicitly calculated as $\phi_{\mathbf{a}\mathbf{b}}(\xi) = \phi_{\mathbf{b}} \circ \phi_{\mathbf{a}}^{-1}(\xi) = J_2 R_{\mathbf{b}} \frac{R_{\mathbf{a}}^{\top}(J_2^{\top}\xi + \mathbf{e}_3)/\sqrt{\xi^{\top}\xi + 1}}{\mathbf{b}^{\top} R_{\mathbf{a}}^{\top}(J_2^{\top}\xi + \mathbf{e}_3)/\sqrt{\xi^{\top}\xi + 1}} = J_2 R_{\mathbf{b}} R_{\mathbf{a}}^{\top} \frac{J_2^{\top}\xi + \mathbf{e}_3}{\mathbf{b}^{\top} R_{\mathbf{a}}^{\top}(J_2^{\top}\xi + \mathbf{e}_3)}$. For all $\xi \in \phi_{\mathbf{a}}(U_{\mathbf{a}} \cap U_{\mathbf{b}})$, $R_{\mathbf{a}}^{\top}(J_2^{\top}\xi + \mathbf{e}_3)$ is parallel to $\phi_{\mathbf{a}}^{-1}(\xi)$ in view of (3). Note that $\phi_{\mathbf{a}}^{-1}(\xi)$ lies in $U_{\mathbf{a}} \cap U_{\mathbf{b}}$, thus $\mathbf{b}^{\top} \phi_{\mathbf{a}}^{-1}(\xi) > 0$, which further implies that $\mathbf{b}^{\top} R_{\mathbf{a}}^{\top}(J_2^{\top}\xi + \mathbf{e}_3) > 0$. Thus $\phi_{\mathbf{a}\mathbf{b}}(\xi)$ is well-defined. To show the smoothness of $\phi_{\mathbf{a}\mathbf{b}}$, re-denote $\phi_{\mathbf{a}\mathbf{b}}(\xi) := \frac{C^{\top}\xi + \mathbf{d}}{\mathbf{f}^{\top}\xi + g}$ with the constant parameters $C := J_2 R_{\mathbf{b}} R_{\mathbf{a}}^{\top} J_2^{\top}$, $\mathbf{d} := J_2 R_{\mathbf{b}} R_{\mathbf{a}}^{\top} \mathbf{e}_3$, $\mathbf{f} := \mathbf{b}^{\top} R_{\mathbf{a}}^{\top} J_2^{\top}$, $g := \mathbf{b}^{\top} R_{\mathbf{a}}^{\top} \mathbf{e}_3$. The nominator and the denominator are thus smooth functions of ξ . Further noticing that the denominator of the n -th derivative $(\mathbf{f}^{\top}\xi + g)^{n+1} > 0$, $n \in \mathbb{N}$ (due to the fact that $\mathbf{f}^{\top}\xi + g > 0$), we have $\phi_{\mathbf{a}\mathbf{b}}(\cdot)$ is a smooth diffeomorphism. Thus a collection of charts $\mathcal{A} = \{(U_{\mathbf{a}}, \phi_{\mathbf{a}})\}_{\mathbf{a} \in \mathbb{S}^2}$ is a smooth atlas for \mathbb{S}^2 . \square

REFERENCES

- [1] F. Bullo, R. Murray, A. Sarti *et al.*, "Control on the sphere and reduced attitude stabilization," in *Third IFAC Symposium on Nonlinear Control Systems Design*, 1995, pp. 495–501.
- [2] P. Tsiotras, M. Corless, and J. Longuski, "A novel approach to the attitude control of axisymmetric spacecraft subject to two control torques," *Automatica*, vol. 31, no. 8, pp. 1099–1112, 1995.
- [3] A. S. Shiriaev, H. Ludvigsen, and O. Egeland, "Swinging up the spherical pendulum via stabilization of its first integrals," *Automatica*, vol. 40, no. 1, pp. 73–85, 2004.
- [4] M. Ramp and E. Papadopoulos, "Attitude and angular velocity tracking for a rigid body using geometric methods on the two-sphere," in *2015 European Control Conference (ECC)*, 2015, pp. 3238–3243.
- [5] S. P. Bhat and D. S. Bernstein, "A topological obstruction to continuous global stabilization of rotational motion and the unwinding phenomenon," *Systems and Control Letters*, vol. 39, pp. 63–70, 2000.
- [6] T. Lee, M. Leok, and N. H. McClamroch, "Stable manifolds of saddle equilibria for pendulum dynamics on \mathbb{S}^2 and \mathbb{S}^3 ," in *2011 50th IEEE Conference on Decision and Control and European Control Conference*. IEEE, 2011, pp. 3915–3921.
- [7] H. B. Hablani, "Attitude commands avoiding bright objects and maintaining communication with ground station," *Journal of Guidance, Control, and Dynamics*, vol. 22, no. 6, pp. 759–767, 1999.
- [8] U. Lee and M. Mesbahi, "Feedback control for spacecraft reorientation under attitude constraints via convex potentials," *IEEE Transactions on Aerospace and Electronic Systems*, vol. 50, pp. 2578–2592, 2014.
- [9] H. C. Kjellberg and E. G. Lightsey, "Discretized quaternion constrained attitude pathfinding," *Journal of Guidance, Control, and Dynamics*, vol. 38, no. 11, pp. 713–718, 2015.
- [10] X. Tan, S. Berkane, and D. V. Dimarogonas, "Constrained attitude maneuvers on $SO(3)$: Rotation space sampling, planning and low-level control," *Automatica*, vol. 112, 2020.
- [11] G. Wu and K. Sreenath, "Safety-critical and constrained geometric control synthesis using control lyapunov and control barrier functions for systems evolving on manifolds," in *2015 American Control Conference (ACC)*, 2015, pp. 2038–2044.
- [12] S. Berkane and D. V. Dimarogonas, "Constrained stabilization on the n -sphere," *arXiv*, 2019. [Online]. Available: <http://arxiv.org/abs/1910.01498>
- [13] M. K. Helwa and M. E. Broucke, "Monotonic reach control on polytopes," *IEEE Transactions on Automatic Control*, vol. 58, no. 10, pp. 2704–2709, 2013.
- [14] S. R. Lindemann and S. M. LaValle, "Simple and efficient algorithms for computing smooth, collision-free feedback laws over given cell decompositions," *The International Journal of Robotics Research*, vol. 28, no. 5, pp. 600–621, 2009.
- [15] J. Ratcliffe, *Foundations of hyperbolic manifolds*. Springer Science & Business Media, 2006, vol. 149.
- [16] H. S. M. Coxeter, *Introduction to geometry*. Wiley classics library, 1969.
- [17] D. S. Bernstein, *Matrix Mathematics: Theory, Facts, and Formulas*. Princeton university press, 2009.